Link between antiferromagnetism and superconductivity probed by nuclear spin relaxation in organic conductors

C. Bourbonnais[1,2] and A. Sedeki[1]
[1]*Département de Physique, Regroupement Québecois sur les Matériaux de Pointe, Université de Sherbrooke, Sherbrooke, Québec, Canada J1K-2R1*
[2]*Canadian Institute for Advanced Research, Toronto, Ontario, Canada M5G 1Z8*
(Received 17 May 2009; published 11 August 2009)

The interdependence of antiferromagnetism and superconductivity in the Bechgaard salts series of organic conductors is examined in the light of the anomalous temperature dependence of the nuclear spin-lattice relaxation rate. We apply the renormalization-group approach to the electron gas model to show that the crossover from antiferromagnetism to superconductivity along with the anomalous nuclear relaxation rate of the Bechgaard salts can be well described within a unified microscopic framework. For sizable nesting deviations of the Fermi surface, scaling theory reveals how pairing correlations enhance short-range antiferromagnetic correlations via magnetic Umklapp scattering over a large part of the metallic phase that precedes superconductivity. These enhanced magnetic correlations are responsible for the Curie-Weiss behavior observed in the NMR relaxation rate.

DOI: 10.1103/PhysRevB.80.085105 PACS number(s): 74.20.Mn, 74.70.Kn, 76.60.Es

I. INTRODUCTION

In the attempt to understand how itinerant antiferromagnetism can give rise to superconductivity in correlated electron systems, one faces the difficulty of linking the behavior of spin fluctuations that can be extracted from experiments to the mechanism of pairing that leads to superconductivity. This work is about the quest of such a connection in the Bechgaard salts $[(TMTSF)_2X]$ series of organic conductors. We ground our analysis on scaling theory, which allows a re-examination of the nuclear spin relaxation in the metallic phase of these low-dimensional molecular systems.

The $(TMTSF)_2X$ compounds are quasi-one-dimensional (quasi-1D) conductors known to exhibit a spin-density-wave (SDW) state adjacent to superconductivity (SC) in their phase diagram.[1–3] This particular sequence of states is achieved by the application of hydrostatic pressure or by chemical means from anion X substitution. Among the host of experimental tools used to study this pattern of phases, the nuclear magnetic resonance (NMR) technique takes on particular importance due to its sensitivity to spin correlations.[4–9] In the metallic state of the SC side of the phase diagram, NMR measurements have revealed the existence of an anomalous enhancement of the nuclear spin-lattice relaxation rate T_1^{-1}. The enhancement was first observed for the ambient pressure superconductor $(TMTSF)_2ClO_4$,[4,10,11] and subsequently found by different groups to be a common characteristic of the series in the metallic state above the critical pressure for superconductivity.[5,7–9] The T_1^{-1} temperature profile shows pronounced deviations from the Korringa law, $T_1^{-1} \propto T$, which is normally expected in conventional metals. These deviations were originally ascribed to the presence of short-range antiferromagnetic spin fluctuations extending in temperature dozens of times the superconducting $T_c \sim 1$ K in the metallic state.[4] The amplitude of the deviations are strongly pressure dependent and seemingly tied to the amplitude of T_c,[3,5,12] suggesting that antiferromagnetism and Cooper pairing are closely related.

It was initially proposed that one-dimensional short-range antiferromagnetic correlations are a key determinant in the enhancement of T_1^{-1}. This low-dimensional response was shown to ultimately crossover into a higher dimensional metallic phase around 10 K, below which a Korringa law was predicted to be recovered.[4] However, the dimensional aspects of such an interpretation run into difficulties when one compares the temperature scale for the crossover to the range of values otherwise extracted from experiments,[13–15] and which would rather place this scale an order of magnitude higher in temperature. An additional defect comes from an important observation made by Brown *et al.*,[3] concerning the temperature profile of the relaxation. Based on the analysis of recent measurements,[3,8,9] it was shown that the Korringa behavior is in effect not recovered down to the lowest temperature preceding superconductivity. Deviations actually persist indicating that staggered spin fluctuations, though nonsingular, keep growing as the temperature is lowered, imposing a Curie-Weiss (CW) temperature dependence for the relaxation rate. Noticeably enough, however, the characteristics of the CW response persists down to T_c and the amplitude of the anomaly as a whole evolves rapidly under pressure like the temperature scale for the onset of superconductivity. The question then arises if, in accordance with the customary view, a sharp distinction can be drawn between both phenomena, or if they are in effect dynamically linked, a possibility that would not only connect magnetism to superconductivity but also involve superconductive pairing in the enhancement of spin correlations.

It is from the latter perspective that we shall reconsider the T_1^{-1} problem for the Bechgaard salts.[16] This will be achieved with the help of the weak coupling renormalization-group (RG) theory.[17,18] Recent developments along these lines have demonstrated how the one-loop RG can take into account density wave and Cooper pairings

on equal footing in correlated quasi-1D metals. In the framework of the repulsive quasi-1D electron gas model, it was found that unconventional singlet "d-wave" (SCd) or in certain conditions triplet "f-wave" superconductivity can be dynamically generated next to a SDW state as alterations of the nesting of the Fermi surface—which mimic pressure effect—are made sufficiently large. From a similar approach to be brought forward here, a CW-type behavior for the spin-fluctuation response is shown to take place over a large temperature interval above T_c within a SCd scenario. It originates from magnetic Umklapp scattering whose amplitude is apparently strengthened by constructive interference with superconductive pairing. The amplitude of spin correlations rapidly decline under "pressure," in line with the decrease in T_c. When transposed into a T_1^{-1} calculation, the RG results can give a satisfactory account of the key features shown by the nuclear relaxation rate, establishing a direct connexion between spin fluctuations and the mechanism of superconductivity in the Bechgaard salts.

In Sec. II we introduce the quasi-1D electron-gas model in the presence of weak Umklapp scattering and alteration of nesting. We review the results of the three-variables RG method obtained at the one-loop level within a SDW-SCd scenario. The temperature profile of the antiferromagnetic and superconducting responses are given and scrutinized as a function of nesting deviations of the Fermi surface. The temperature scales are extracted and used to construct the phase diagram of the model. In Sec. III, the explicit form for T_1^{-1} is calculated from the RG results for both the antiferromagnetic and uniform components of spin fluctuations. In Sec. IV we discuss the results and conclude.

II. ITINERANT ANTIFERROMAGNETISM AND SUPERCONDUCTIVITY: RENORMALIZATION-GROUP RESULTS

We consider the electron-gas model[18–21] whose bare Hamiltonian for a square lattice of $N_\perp \times N_\perp$ chains of length L is given by

$$
\begin{aligned}
H = & \sum_{p,\mathbf{k},\sigma} E_p(\mathbf{k}) c^\dagger_{p,\mathbf{k},\sigma} c_{p,\mathbf{k},\sigma} \\
& + \frac{1}{LN_\perp^2} \sum_{\{\mathbf{k},\sigma\}} [g_1 c^\dagger_{+,\mathbf{k}'_1,\sigma_1} c^\dagger_{-,\mathbf{k}'_2,\sigma_2} c_{+,\mathbf{k}_2,\sigma_2} c_{-,\mathbf{k}_1,\sigma_1} \\
& + g_2 c^\dagger_{+,\mathbf{k}'_1,\sigma_1} c^\dagger_{-,\mathbf{k}'_2,\sigma_2} c_{-,\mathbf{k}_2,\sigma_2} c_{+,\mathbf{k}_1,\sigma_1} \\
& + g_3 (c^\dagger_{+,\mathbf{k}'_1,\sigma_1} c^\dagger_{+,\mathbf{k}'_2,\sigma_2} c_{-,\mathbf{k}_2,\sigma_2} c_{-,\mathbf{k}_1,\sigma_1} \\
& + \text{H.c.})] \delta_{\mathbf{k}_1+\mathbf{k}_2=\mathbf{k}'_1+\mathbf{k}'_2(\pm\mathbf{G})},
\end{aligned} \tag{1}
$$

where the operator $c^\dagger_{p,\mathbf{k},\sigma}(c_{p,\mathbf{k},\sigma})$ creates (destroys) a right ($p=+$) and left ($p=-$) moving electrons of wave vector $\mathbf{k}=(k,k_b,k_c)$ and spin σ. The free part is modeled by the one-electron energy spectrum

$$
\begin{aligned}
E_p(\mathbf{k}) = & v_F(pk - k_F) - 2t_{\perp b}\cos k_b - 2t'_{\perp b}\cos 2k_b \\
& - 2t_{\perp c}\cos k_c,
\end{aligned} \tag{2}
$$

where v_F and k_F are the longitudinal Fermi velocity and wave vector; $t_{\perp b}$ and $t_{\perp c}$ are the nearest-neighbor hopping integrals in the two perpendicular directions. The small transverse second nearest-neighbor hopping $t'_{\perp b} \ll t_{\perp b}$ parameterizes the alteration of nesting of the open Fermi surface, which simulates the most important effect of pressure in our model. The quasi-1D anisotropy of the spectrum is $E_F \simeq 15 t_{\perp b} \simeq 450 t_{\perp c}$, where $E_F = v_F k_F \simeq 3000$ K is the longitudinal Fermi energy congruent with the range found in the Bechgaard salts;[22–24] E_F is half the bandwidth $E_0 = 2E_F$ in the model. The interacting part of the Hamiltonian is described by the bare backward (g_1) and forward (g_2) scattering amplitudes between right and left moving electrons. In terms of the extended Hubbard model parameters, $g_1 = U - 2V$ and $g_2 = U + 2V$, where U and V are the on-site and nearest-neighbor repulsions. The half-filling character of the band—due to the small dimerization of the chains—gives rise to Umklapp scattering of bare amplitude g_3,[20] for which momentum conservation is satisfied modulo the longitudinal reciprocal lattice vector $\mathbf{G} = (4k_F, 0, 0)$.

In the repulsive sector, the couplings satisfy $g_1 - 2g_2 < g_3$, a condition that promotes antiferromagnetic spin fluctuations in the presence of nesting. In spite of a variety of possibilities for the couplings that would be generic for the phenomena we want to discuss, one can call upon experiments and band calculations to delimit their range and make a choice for the amplitude of normalized couplings $\tilde{g}_i \equiv g_i / \pi v_F$ for the calculations that will follow. We first note that—half-filling—Umklapp term $\tilde{g}_3 \approx \frac{\Delta_D}{E_F} \tilde{g}_1$ is proportional to a small dimerization gap Δ_D due to the modulation of the electron transfer integral along the stacks.[20,25,26] For $(TMTSF)_2X$ compounds, the modulation is relatively small and one finds $\frac{\Delta_D}{E_F} \lesssim 0.1$.[22–24] The backscattering coupling $\tilde{g}_1$ governs spin excitations and is involved in the enhancement of static spin susceptibility.[27,28] Experiments in the Bechgaard salts indicate that this enhancement is around 20% the noninteracting band value at low temperature.[7,29,30] This is compatible with the use of a bare backscattering amplitude in the interval $\tilde{g}_1 \simeq 0.3, \ldots, 0.5$, giving in turn the range $\tilde{g}_3 \simeq 0.02, \ldots, 0.04$ for Umklapp. As for the forward scattering, its bare amplitude can be adjusted in order for the calculated temperature scale for SDW ordering to fall in the range of observed values 10–20 K at moderate nesting frustration. This leads to $\tilde{g}_2 \simeq 0.5, \ldots, 0.7$. Though nonexhaustive, this range of parameters is found to be generic of the interdependence between magnetism and superconductivity. The RG calculations, that follow, have been carried out for $\tilde{g}_1 = 0.32$, $\tilde{g}_2 = 0.64$, and $\tilde{g}_3 = 0.02$.

The RG method consists of integrating successively the degrees of freedom from the high energy cutoff E_F down to the energy $\frac{1}{2}E_0(\ell) = \frac{1}{2}E_0 e^{-\ell}$ above and below the Fermi sheets at step ℓ. At the one-loop level, the corrections to the amplitudes $\tilde{g}_i$ as a function of ℓ come from the electron-electron (Cooper) and electron-hole (Peierls) scattering channels. Both interfere and generate momentum dependence for the scattering amplitudes as $E_0(\ell) = E_0 e^{-\ell}$ is reduced with increasing ℓ. Here the influence on the RG flow of the smallest

transverse hopping integral, $t_{\perp c}$, is negligible and has been ignored. In the three momentum variables scheme of the renormalization-group adopted here,[18] each sheet of the Fermi surface is divided into 32 pieces or patches whose location defines a particular transverse momentum k_b in the b direction. Only the k_b dependence is retained for the couplings, which becomes $g_i \to g_i(k'_{b1}, k'_{b2}; k_{b2}, k_{b1})$. The explicit form of the corresponding flow equations has been given previously [Eqs. Eqs. (10)–(12) of Ref. 18] and these need not to be repeated here.

Following their integration up to $\ell \to \infty$, the presence of a singularity in the scattering amplitudes signals an instability of the normal state at a "critical" temperature T_μ.[31] To see what kind of order it refers to, we compute the susceptibilities. For the intrachain interactions given above, a singularity has been shown to occur either in the static μ=SDW or the SCd susceptibility χ_μ.[17,18] In the RG framework, these are expressed as a loop integration

$$\chi_\mu(\mathbf{q},\omega) = \frac{1}{\pi v_F}\int_0^{\tilde{\chi}^0_\mu(\mathbf{q},\omega)} \langle f_\mu(k_b) z^2_\mu(k_b)\rangle d\ell, \tag{3}$$

where $\langle \cdots \rangle$ is an average over k_b, $f_\mu(k_b)=1(\cos k_b)$ is a form factor for the μ=SDW (SCd) order parameters; $z_\mu(k_b)$ is the scaling factor associated to the response function of the channel μ and which will be defined shortly. In the T_1^{-1} analysis given in Sec. III A, the dependence on the (real) frequency ω and the three-dimensional wave vector $\mathbf{q}=(q,q_b,q_c)$ of $\chi_{\rm SDW}$ is needed. It can be introduced through the upper bound of the loop integration, which will be taken as the normalized free-electron dynamic susceptibility $\tilde{\chi}^0_\mu = \pi v_F \chi^0_\mu$ of the SDW channel

$$\tilde{\chi}^0_{\rm SDW}(\mathbf{q}_0+\mathbf{q},\omega) = \ln\frac{E_F}{T} + \psi\left(\frac{1}{2}\right) - \frac{1}{8\pi^2}\int_{-\pi}^{+\pi}\int_{-\pi}^{+\pi} dk_b dk_c \left[\psi\left(\frac{1}{2} + i\frac{\xi_{\rm P}(\mathbf{k}_\perp,\mathbf{q},\omega)}{4\pi T}\right) + \text{c.c.}\right]. \tag{4}$$

$\tilde{\chi}^0_{\rm SDW}$ has been expressed in terms of the deviations $\mathbf{q}$ to the best nesting vector $\mathbf{q}_0=(2k_F,\pi,\pi)$. Here $\psi(x)$ is the digamma function and

$$\xi_{\rm P}(\mathbf{k}_\perp,\mathbf{q},\omega) \simeq v_F q + (2t_{\perp b}\sin k_b) q_b - 4t'_{\perp b}\cos 2k_b + (2t_{\perp c}\sin k_c)\sin q_c - \omega. \tag{5}$$

As for $\chi_{\rm SCd}$ in the Cooper channel, it will be evaluated in the uniform $\mathbf{q}=0$ and static $\omega=0$ limit, where $\tilde{\chi}^0_{\rm SCd} = \ln E_F/T$.

Following Ref. 18, the flow equation for the static SDW vertex part at $(2k_F,\pi)$ is given by

$$\partial_\ell z_{\rm SDW}(k_b) = \frac{1}{2\pi}\int_{-\pi}^{+\pi} d\bar{k}_b B_P(\bar{k}_b) z_{\rm SDW}(\bar{k}_b) \times [g_2(\bar{k}_b + \pi, k_b, \bar{k}_b, k_b+\pi) + g_3(\bar{k}_b, k_b, \bar{k}_b+\pi, k_b+\pi)], \tag{6}$$

which is governed by the combination of couplings g_2+g_3. For the static $\chi_{\rm SCd}$, one has $f_{\rm SCd}(k_b)=\cos k_b$ for the form factor and the vertex part at zero pair momentum obeys to

$$\partial_\ell z_{\rm SCd}(k_b) = -\frac{1}{2\pi}\int_{-\pi}^{+\pi} d\bar{k}_b B_C(\bar{k}_b) z_{\rm SCd}(\bar{k}_b) \times [g_1(\bar{k}_b, -\bar{k}_b, k_b, -k_b) + g_2(\bar{k}_b, -\bar{k}_b, -k_b, k_b)], \tag{7}$$

which is governed by the combination $-g_1-g_2$. The above expressions depend on the ℓ derivative of the Peierls and Cooper loops which read

$$B_{\rm P/C}(\bar{k}_b) = \sum_{\nu=\pm 1} \theta[|E_0(\ell)/2 + \nu A_{\rm P/C}(\bar{k}_b)| - E_0(\ell)/2] \times \frac{1}{2}\left[\tanh\frac{E_0(\ell)/2 + \nu A_{\rm P/C}(\bar{k}_b)}{2T} + \tanh\frac{E_0(\ell)}{4T}\right] \times \frac{E_0(\ell)/2}{E_0(\ell) + \nu A_{\rm P/C}(\bar{k}_b)}, \tag{8}$$

where $A_{\rm P}(\bar{k}_b)=4t'_{\perp b}\cos 2k_b$, $A_{\rm C}=0$, and $\theta(x)$ is the step function with the definition $\theta(0)\equiv\frac{1}{2}$.

The RG results at the one-loop level for the temperature dependence of the normalized $\tilde{\chi}_{\rm SDW}$ and $\tilde{\chi}_{\rm SCd}(\tilde{\chi}_\mu \equiv \pi v_F \chi_\mu)$ are given in Fig. 1 for different values of the nesting frustration parameter $t'_{\perp b}$. At small $t'_{\perp b}$, $\tilde{\chi}_{\rm SDW}$ diverges signaling an instability toward the formation of a SDW state at the temperature $T_{\rm SDW}$. This scale decreases as $t'_{\perp b}$ is raised and at the approach of the threshold $t'^*_{\perp b}\simeq 25.6$ K (for the set of parameters used), it undergoes a rapid drop. However, $T_{\rm SDW}$ does not go to zero, but is replaced by another scale T_c at which $\tilde{\chi}_{\rm SCd}$ is singular and an instability of the metallic state against d-wave superconductivity takes place. This yields a maximum in T_c when $T_{\rm SDW}$ is minimum, namely, where the coupling strength, mediated by spin fluctuations, is maximum. When $t'_{\perp b}$ is further raised, T_c decreases monotonically. The overall variation in the temperature scale for the metallic state instability of Fig. 1(b) captures fairly well the characteristic variation in the critical temperature found in compounds such as $(TMTSF)_2X$ under pressure.[1–3]

The temperature dependence of $\tilde{\chi}_{\rm SDW}$ is of particular interest. To begin with the region well below $t'^*_{\perp b}$, on the SDW side, namely, far from the boundary between SCd and SDW, the plot of $\tilde{\chi}^{-1}_{\rm SDW}$ in Fig. 2 shows a linear behavior in temperature down to $T_{\rm SDW}$, which is characteristic of a $(T-T_{\rm SDW})^{-\gamma}$ singularity for $\tilde{\chi}_{\rm SDW}$ with the classical exponent $\gamma=1$. As the boundary is approached, however, this behavior for $\tilde{\chi}^{-1}_{\rm SDW}$ does not extend down to the critical point, but

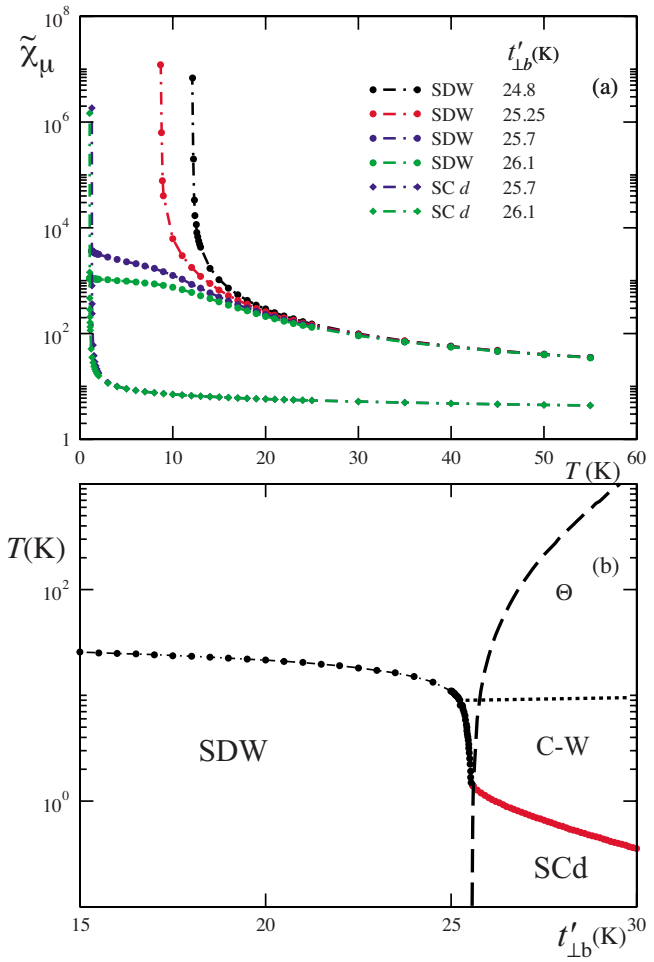

FIG. 1. (Color online) (a) Temperature variation in the normalized static susceptibility $\tilde{\chi}_\mu$ in the SDW and SCd channels at various $t'_{\perp b}$ on either side of the threshold value $t'^{*}_{\perp b}$; (b) RG phase diagram of the quasi-1D electron-gas model (see text). The dashed line stands as the CW scale Θ in the superconducting sector. The dotted line defines the temperature domain of the CW behavior.

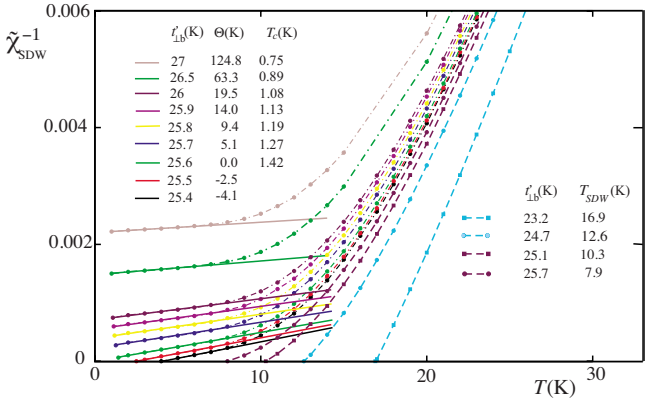

FIG. 2. (Color online) Calculated inverse normalized SDW susceptibility as a function of temperature for different $t'_{\perp b}$. The continuous lines correspond to the Curie-Weiss regime.

evolves toward another regime as deterioration of nesting conditions becomes more perceptible and $T_{\rm SDW}$ decreases rapidly. By inspection, the latter regime for $\tilde{\chi}^{-1}_{\rm SDW}$ is also found to be linear sufficiently close to $T_{\rm SDW}$, but with a smaller slope. The temperature interval above $T_{\rm SDW}$, where it takes place, increases as $t'_{\perp b}$ grows. This regime, which we parameterize by a CW form $\tilde{\chi}^{-1}_{\rm SDW}=C(T+\Theta)$, has a negative scale Θ that coincides with $T_{\rm SDW}$ at $t'_{\perp b}\lesssim t'^{*}_{\perp b}$.

As one reaches $t'_{\perp b}=t'^{*}_{\perp b}$ where the system is superconducting, $\Theta=0$ and $\tilde{\chi}_{\rm SDW}\sim 1/T$. If superconductivity was absent the system would be then quantum critical in the SDW channel with a singular antiferromagnetic correlation length $\xi_{a,b}\sim T^{-\nu}$, of exponent $\nu=1/2$ in the ab plane. As for the dynamical exponent z, the results of Sec. III give $z=2$. The CW form carries on in the superconducting sector where Θ becomes positive and grows with $t'_{\perp b}$. Since $\tilde{\chi}(T\to 0)\to 1/C\Theta$, the amplitude of Θ is thus connected to the size of spin fluctuations in the low-temperature limit, which decreases rapidly with $t'_{\perp b}$. It follows that $\tilde{\chi}_{\rm SDW}$, though no longer singular above $t'^{*}_{\perp b}$, is still temperature dependent: despite altered nesting conditions and scaling toward the formation of a singlet superconducting ground state, antiferromagnetic correlations continue to grow down to T_c. The CW behavior extends several times T_c in the metallic state.

The existence of a CW behavior above $t'^{*}_{\perp b}$ is intimately linked to the presence of magnetic Umklapp scattering (g_3) in the model; without this coupling, $\tilde{\chi}_{\rm SDW}$ is essentially flat at low temperature. This is confirmed by putting $g_3=0$ and carrying out the calculation with the remaining coupling constants. Most surprisingly, however, strongly reduced nesting of the Fermi surface alone plays little role in the enhancement of Umklapp. The augmentation turns out to be a consequence of Cooper SCd pairing that reinforces spin fluctuations in the metallic state. This can be easily checked by setting $B_C=0$, which removes all the Cooper pairing terms from the flow equations of the coupling constants. In this superconductive pairingfree scheme, which is equivalent to a ladder diagrammatic (mean-field) summation in the density-wave pairing channel alone, the CW behavior is negligible for $t'_{\perp b}\geq t'^{*}_{\perp b}$.

Interestingly enough, Umklapp scattering is coupled to g_1 and g_2, which both flow to strong coupling at the approach of the superconductive fixed point at T_c. At variance with ordinary s-wave superconductivity,[32] these scattering amplitudes are momentum dependent in a SCd scenario yielding an overall positive sign for their coupling with Umklapp. It follows that the singular growth of SCd pairing at low temperature [Fig. 1(a)] interferes positively with Umklapp expanding the temperature range where this coupling and, in turn, spin fluctuations increase. It is this self-consistency between the two pairing channels that is responsible for the CW law for the staggered magnetic susceptibility down to T_c. It is worth stressing that the reinforcement of the SDW channel is not limited to the SC sector, but is also manifest for $t'_{\perp b}\lesssim t'^{*}_{\perp b}$, where the CW behavior, with a negative Θ, is indicative of a SDW instability driven by Cooper pairing.

III. NUCLEAR SPIN-LATTICE RELAXATION RATE

A. Theoretical prediction for the staggered and uniform contributions to nuclear relaxation

We now turn to the derivation of the nuclear relaxation rate in the RG scheme. The T_1^{-1} calculation starts from the Moriya expression[33]

$$T_1^{-1} = T\int |A_{\mathbf{q}}|^2 \frac{\chi''(\mathbf{q},\omega)}{\omega} d^3q, \tag{9}$$

which relates T_1^{-1} to the imaginary part of the retarded spin susceptibility χ''. Here $A_{\mathbf{q}}$ is proportional to the hyperfine matrix element. The integral over all $\mathbf{q}$ indicates that T_1^{-1} is sensitive to staggered and uniform electronic spin correlations with, respectively, large $\mathbf{q}\sim\mathbf{q}_0$ and small parallel $q \sim 0$. We then consider the following decomposition:

$$T_1^{-1} = T\left(\int_{q\sim 0} + \int_{\mathbf{q}\sim\mathbf{q}_0}\right)|A_{\mathbf{q}}|^2 \frac{\chi''(\mathbf{q},\omega)}{\omega} d^3q, \equiv T_1^{-1}(q\sim 0) + T_1^{-1}(\mathbf{q}_0). \tag{10}$$

Let us first examine the staggered component, $T_1^{-1}(\mathbf{q}_0)$. Using Eqs. (3) and (4), the expression of $\chi''(\mathbf{q}+\mathbf{q}_0,\omega)$ at small $\mathbf{q}$ and ω is given by

$$\mathrm{Im}\,\chi_{\mathrm{SDW}}(\mathbf{q}+\mathbf{q}_0,\omega) = \frac{\chi_{\mathrm{SDW}}(\mathbf{q}_0)\Gamma\omega}{[1+\xi_a^2q^2+\xi_b^2q_b^2+\xi_c^2(\sin q_c)^2]^2+\Gamma^2\omega^2}. \tag{11}$$

From the results of the Appendix, $\xi_i^2 = \xi_{0,i}^2\langle z_{\mathrm{SDW}}^2(k_b)\rangle/\tilde{\chi}_{\mathrm{SDW}}$ is the squared of the correlation length along $i=a$, b, and c directions; $\xi_{0,a}\propto v_F/T_0$ and $\xi_{0,b,c}\propto t_{\perp b,c}/T_0$ are the corresponding coherence lengths evaluated at the SDW temperature $T_0\simeq 12$ K obtained at small $t'_{\perp b}$; $\Gamma = \Gamma_0\langle z_{\mathrm{SDW}}^2(k_b)\rangle/\tilde{\chi}_{\mathrm{SDW}}$ is the relaxation time for SDW fluctuations and $\Gamma_0\propto 1/T_0$ is a characteristic short-range time scale. The integration over $\mathbf{q}$ is carried out in Appendix and yields

$$T_1^{-1}(\mathbf{q}_0) = 2\pi^3|A_{q_0}|^2[N(E_F)]^2 v_F\Gamma_0/(\xi_{0,a}\xi_{0,b}) \times T\tilde{\chi}_{\mathrm{SDW}}\left[\frac{1}{\sqrt{1+\xi_c^2}} - \frac{1}{\sqrt{(1+r)(1+r+\xi_c^2)}}\right], \tag{12}$$

where $r\simeq 1.114\langle z_{\mathrm{SDW}}^2(k_b)\rangle/\tilde{\chi}_{\mathrm{SDW}}$ and $N(E_F)=1/\pi v_F$ corresponds to the density of states at the Fermi level. The enhancement of the staggered component as the temperature is lowered is thus connected to the static SDW response which can be obtained by the RG method.

We next consider the uniform component of the relaxation rate which is connected to the imaginary part of the dynamic spin susceptibility at small ω and q. In this limit, $\chi(\mathbf{q},\omega)$ has been shown to be nonsingularly enhanced by interactions at low temperature.[7,27,28] Within the random-phase approximation (RPA), the expression of the imaginary part reads

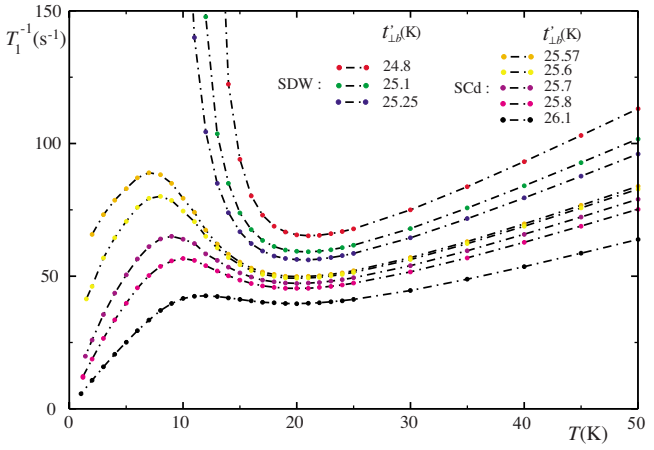

FIG. 3. (Color online) Calculated temperature profile of nuclear relaxation rate as a function of temperature for $t'_{\perp b}$ below and above the threshold value $t'^{*}_{\perp b}$.

$$\chi''(\mathbf{q},\omega)|_{\omega,q\to 0} = -\eta^2\frac{1}{4\pi^3}\sum_p \int dk dk_b dk_c \{n[E_p(\mathbf{k}+\mathbf{q})] - n[E_p(\mathbf{k})]\}\delta[\omega - E_p(\mathbf{k}+\mathbf{q}) + E_p(\mathbf{k})], \tag{13}$$

where $n(x)$ is the Fermi distribution. The uniform contribution for the imaginary part is enhanced from electron-electron interaction by the factor η (see Appendix). From previous measurements of the static and uniform spin susceptibility,[29,30] its enhancement is about 20% in the low-temperature domain so that the factor can be fixed to $\eta \simeq 1.2$ considered as temperature independent in the range of interest.[34] Substituting in Eq. (10), the remaining integrals are carried out in the Appendix and lead to the "Korringa" component

$$T_1^{-1}(q\sim 0) = \pi|A_0|^2[N(E_F)]^2\eta^2 T. \tag{14}$$

While the uniform contribution is nonsingular, its amplitude is known to become ultimately larger than the staggered component at high enough temperature.[27]

B. Results and relation to experiments

To compare the sum of Eqs. (12) and (14), as the calculated T_1^{-1} (Fig. 3), with the experimental findings for ^{77}Se T_1^{-1} in $(TMTSF)_2PF_6$ and $(TMTSF)_2ClO_4$ (Refs. 4 and 5), we adjust the two unknown constants $|A_0|$ and $|A_{\mathbf{q}_0}|$ so that the amplitude of T_1^{-1} falls in the range of the observed values (Fig. 4). Since in the high-temperature region, the nuclear relaxation rate is dominated by the uniform contribution,[7,35] $|A_0|$ is adjusted to make $T_1^{-1}(q\sim 0)$ matching with the measured T_1^{-1} values at 50 K. The other constant $|A_{\mathbf{q}_0}|$ for the staggered part is tuned such that T_1^{-1} is congruent with the measured value at 20 K. A ratio of $|A_{\mathbf{q}_0}|/|A_0|\sim 10^{-2}$ is thus found for the hyperfine matrix elements.[36] The total expression of T_1^{-1} is then plotted in Fig. 3 for various values of the nesting frustration parameter $t'_{\perp b}$, namely, below and above the threshold for superconductivity in the calculated phase diagram of Fig. 1(b).

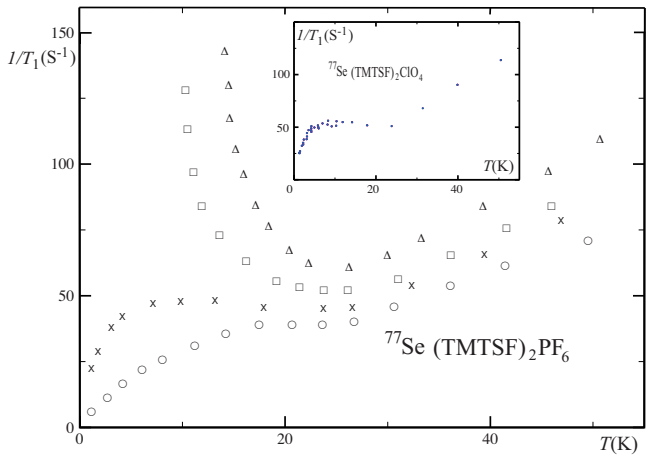

FIG. 4. (Color online) ^{77}Se T_1^{-1} vs temperature measured in $(TMTSF)_2PF_6$ in the SDW regime at $P=1$ bar (triangles), 5.5 kbar (squares) and in SC regime at $P=8$ kbar (crosses) and 11 kbar (circles) (Ref. 5). Inset: ^{77}Se T_1^{-1} vs T in $(TMTSF)_2ClO_4$ at $P=1$ bar (Refs. 4 and 10).

In the SDW domain for $t'_{\perp b} \leq t'^{*}_{\perp b}$, the relaxation rate Eq. (12) behaves as $T_1^{-1} \propto T\tilde{\chi}_{\mathrm{SDW}}/\sqrt{1+\xi_c^2}$ at large r, namely, close to T_{SDW}, where it is dominated by the staggered contribution. The latter then develops a three-dimensional singularity of the form $T^{-1} \sim (T-T_{\mathrm{SDW}})^{-\nu}$, with $\nu=1/2$ when ξ_c becomes large as $T \to T_{\mathrm{SDW}}$. The power-law exponent agrees with the one of mean-field theory in three dimensions.[27] This has been shown long ago to agree with the $(TMTSF)_2PF_6$ data of Fig. 4.[5,7] As one moves away from T_{SDW} in temperature, ξ_c becomes smaller and the system evolves toward a two-dimensional (2D) behavior where $T^{-1} \sim T\tilde{\chi}_{\mathrm{SDW}}$, corresponding to $\nu=1$.

Now if one moves along the $t'_{\perp b}$ scale, by approaching $t'^{*}_{\perp b}$ from below, one enters into a transitional regime where T_{SDW} is relatively small; ξ_c then becomes large and three-dimensional order, with $\nu=1/2$, develops only in very close proximity to the critical point. For $t'_{\perp b} > t'^{*}_{\perp b}$ on the SCd side, T_1^{-1} is no longer singular but shows a pronounced anomaly due to short-range spin fluctuations. These extend deeply in the normal state up to 20 K or so, above which the uniform component of the relaxation takes over and $T_1^{-1} \propto T$. To the anomaly of T_1^{-1} found down to about 10 K (Fig. 3) corresponds a distinct region of increase in χ_{SDW} [Fig. 1(a)] due to the growth of antiferromagnetic correlations close to SDW ordering. T_1^{-1} passes through maximum near 10 K, whose amplitude, and to a lesser extend its location, is $t'_{\perp b}$ dependent; T_1^{-1} then finally starts to go down at lower temperature until one reaches T_c.

The overall structure of the calculated T_1^{-1} anomaly compares fairly well with the data of Creuzet *et al.*,[5] (Fig. 4) and Brown *et al.*,[3] on $(TMTSF)_2PF_6$ above the critical pressure P_c for superconductivity and on $(TMTSF)_2ClO_4$ at ambient pressure ($>P_c$, inset of Fig. 4).

If one looks more closely at the decrease in the calculated T_1^{-1} below 10 K in Fig. 3, it is found that it deviates from a linear Korringa law as a consequence of the growth of spin fluctuations, responsible for the CW behavior for χ_{SDW} in this temperature range (Fig. 1). To see how these fluctuations mark the relaxation rate, it is instructive to look at the temperature dependence of T_1T shown in Fig. 5. In the left panel of this figure, the three different regimes of the calculated relaxation rate can be identified. In the high-temperature regime T_1T tends to level off, dominated by the uniform component Eq. (14). At lower temperature where T_1T is controlled by the staggered component, two 2D linear regimes, governed by $\xi_{a,b}$, can be singled out and related to those found previously for $1/\tilde{\chi}_{\mathrm{SDW}}$ in Fig. 2. Indeed, in the intermediate temperature range, between 20 and 10K or so, T_1T is weakly affected by nesting alterations and evolves with a steep slope that would extrapolate to a finite critical temperature. However, approaching 10 K, these alterations become more perceptible and the slope of T_1T is reduced and enters in the low-temperature CW regime of the form $T_1T=\mathcal{C}(T+\Theta)$. Following the example of $1/\tilde{\chi}_{\mathrm{SDW}}$ when $t'_{\perp b} \leq t'^{*}_{\perp b}$, $\Theta=-T_{\mathrm{SDW}}$, and T_1T is found to be linear, except in the very close vicinity of T_{SDW}, where ξ_c becomes large. At $t'^{*}_{\perp b}$, Θ vanishes and finally grows positively for $t'_{\perp b} > t'^{*}_{\perp b}$ as T_c decreases. The slope $\mathcal{C}$ diminishes as $t'_{\perp b}$ grows, whereas the product $\mathcal{C}\Theta$, corresponding to the extrapolated zero-temperature intercept of T_1T, increases.

From the NMR work of Creuzet *et al.*,[4,10] (inset of Fig. 4) and from of Shinagawa *et al.*,[9] (Fig. 5, lower panel on the

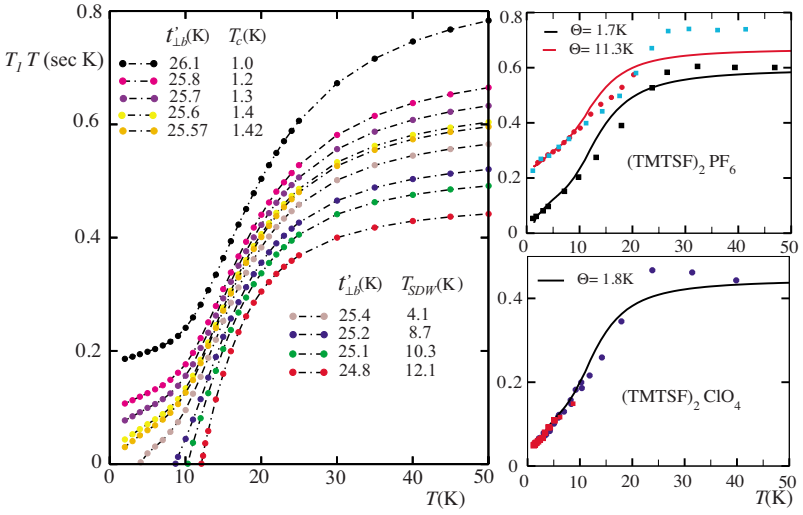

FIG. 5. (Color online) Left: Calculated temperature profile of T_1T for different values of $t'_{\perp b}$ below and above the threshold $t'^{*}_{\perp b}$. Upper right: ^{77}Se T_1T data for $(TMTSF)_2PF_6$ at 9.5 kbar (red (gray) circles, after Wu *et al.*, Ref. 8), 8 kbar, and 11 kbar (green (gray) squares after Creuzet *et al.*, Ref. 5); the continuous lines are theoretical fits (see text). Lower right: ^{77}Se T_1T data for $(TMTSF)_2ClO_4$ at ambient pressure (blue (black) circles, after Creuzet *et al.*, Ref. 4, red (gray) circles, after Shinagawa *et al.*, Ref. 9). The continuous line is a theoretical fit (see text).

right) on $(TMTSF)_2ClO_4$ at ambient pressure, the three regimes of T_1T can be discerned in the data. On the same panel the continuous line corresponds to a fit using the sum of Eqs. (12) and (14), where $|A_{\mathbf{q}_0}| \simeq 18.5$ $(\sec^{-1})$ and $|A_{\mathbf{q}_0}|/|A_0| \simeq 0.7 \times 10^{-2}$, with a CW regime that corresponds to $\Theta \simeq 1.8$ K. In the upper panel of the same figure, the T_1T data of Wu *et al.*[8] and Creuzet *et al.*,[5] (Fig. 4) for $(TMTSF)_2PF_6$ at $P \simeq 10$ kbar are shown. The fit (blue (black) curve) is obtained for $|A_{\mathbf{q}_0}| \simeq 12.8$ $(\sec^{-1})$ and $|A_{\mathbf{q}_0}|/|A_0| \simeq 0.65 \times 10^{-2}$ for which $\Theta \simeq 11.3$ K. For the data on the same compound at 8 kbar, we have $|A_{\mathbf{q}_0}| \simeq 18$ $(\sec^{-1})$ and $|A_{\mathbf{q}_0}|/|A_0| \simeq 0.9 \times 10^{-2}$, with $\Theta \simeq 1.7$ K. The three temperature regimes are revealed from the data at small Θ. However, as pressure increases, in $(TMTSF)_2PF_6$, for example, the temperature interval over which the CW takes place experimentally, apparently increases in size. This pressure effect is not captured by the present calculations for which the CW temperature interval is essentially constant as a function of $t'_{\perp b}$ [Fig. 1(b)]. As for the rapid increase in Θ as the ratio $T_c/T_c(t'^*_{\perp b})$ falls off in Fig. 1(b), it is found to be in fair agreement with the experimental findings in $(TMTSF)_2PF_6$, at least up to moderate pressure where data are available.[3,5]

IV. DISCUSSION AND CONCLUSION

The explanation put forward for the enhancement of spin fluctuations in the metallic state of the $(TMTSF)_2X$ compounds modifies an earlier scheme of interpretation proposed long ago, in which an effective—strongly renormalized—scale for interchain hopping played the dominant part in the temperature profile of the enhancement that was considered one dimensional in character. In the quasi-one-dimensional view adopted here, the coherent wrapping of the open Fermi surface takes place in the temperature domain $\sim t_{\perp b}(\sim 100$ K), that is far above the range where the anomalous features of the relaxation rate are found. It is rather the small parameter $t'_{\perp b}$ for nesting deviations of the whole Fermi surface that acts as the critical parameter and triggers the modification of the relaxation rate in temperature. For repulsive couplings, the increase in $t'_{\perp b}$ alters, as expected, the stability of the SDW fixed point, simulating the effect of pressure.[37,38] At some threshold value $t'^*_{\perp b}$, the SDW fixed point is unstable. However, because of a finite mixing between the weakened density wave and unaltered Cooper pairing singularities in the scattering amplitudes, the electron system is not a Fermi liquid, but is rather characterized by superconducting order, which takes place in the SCd channel for intrachain repulsive interactions.

We have first seen how this crossover between fixed points operates as a function of temperature above $t'^*_{\perp b}$ for the SDW response function. At high temperature, thermal broadening of the Fermi surface makes nesting deviations less perceptible and the electron system is still attracted by the SDW primary fixed point. As the temperature decreases and the fine details of the Fermi surface in the *ab* plane become progressively coherent, the singularity of the SDW response is suppressed. This coincides with the emergence of a secondary SCd fixed point, whose influence stretches in temperature about ten times the maximum T_c value reached at $t'^*_{\perp b}$. Throughout the flow toward T_c, SDW correlations, albeit nonsingular, persist to increase in the *ab* plane, thanks to the strengthening of Umklapp by Cooper SCd pairing. The increase in the SDW susceptibility can be fitted with a Curie-Weiss law in temperature.

The above features found for the susceptibility are also encountered in the antiferromagnetic component of the nuclear relaxation rate as an anomalous enhancement that emerges out of a Korringa or Fermi-liquid-like behavior at low temperature. These characteristics of the nuclear relaxation rate adhere to a large extent to the experimental facts found by NMR in the Bechgaard salts. The relatively rapid evolution of the relaxation rate enhancement seen under pressure, in particular concerning the characteristics of the Curie-Weiss law, can find an explanation in line with the strong reduction in T_c under pressure. This connection between theory and experiment gives significant support to a mechanism of superconductive pairing mediated by spin fluctuations.

As stressed before, at the core of the weak coupling scaling theory resides the finite quantum interference between density-wave and Cooper pairing channels. It gives rise to d-wave superconductivity from the exchange of spin correlations, and conversely to the enhancement of spin correlations from superconductive pairing. This interference is manifest in the one-loop perturbation theory. Higher order effects such as the interaction between SDW modes of fluctuations are neglected. In self-consistent renormalized theory of spin fluctuations where such mode-mode interactions are included,[39] a Curie-Weiss enhancement can be found in the high-temperature part of the normal phase. In such an approach, the SDW channel is singled out and interference with Cooper pairing absent. It follows that CW enhancement does not persist down to the lowest temperature, where instead a Fermi-liquid behavior takes place. Despite this fundamental difference, one cannot exclude that the actual Curie-Weiss enhancement of the nuclear relaxation rate superimposes to some extent both contributions.

In conclusion the above results have highlighted that from a renormalization-group approach to the quasi-one-dimensional electron-gas model, it is possible to obtain a microscopic description of the spin fluctuations, as extracted from nuclear relaxation in $(TMTSF)_2X$. It is through the same approach that the mechanism of interplay between itinerant antiferromagnetism and superconductivity has been worked out for the phase diagram of these compounds.[17,18] In parallel with the work presented here for the relaxation rate, the same approach has been applied to electron transport in the Bechgaard salts, which also shows an anomalous temperature dependence in the metallic state above superconductivity. Calculations of the transport scattering rate are compared to the resistivity in a separate paper.[40]

ACKNOWLEDGMENTS

We thank P. Auban-Senzier, N. Doiron-Leyraud, D. Jérome, L. Taillefer, and A.-M. Tremblay for useful comments on several aspects of this work. C.B. expresses his gratitude to the Natural Sciences and Engineering Research

Council of Canada (NSERC), and the Canadian Institute for Advanced Research (CIFAR) for financial support. The authors are thankful to the Réseau Québécois de Calcul Haute Performance (RQCHP) for supercomputer facilities at the Université de Sherbrooke.

APPENDIX: NUCLEAR RELAXATION RATE

1. Antiferromagnetic part

The wave vector and frequency dependence of the dynamic susceptibility is in general not given by the RG method used here. However, an expression for the imaginary part of the SDW susceptibility can be obtained by restoring the q and ω dependence through the boundary conditions of the flow equation for the susceptibility Eq. (3). Using Eq. (4) at small $\mathbf{q}$ and ω, one finds

$$\begin{aligned}\mathrm{Im}\,\chi_{\mathrm{SDW}}(\mathbf{q}+\mathbf{q}_0,\omega) &= \frac{1}{\pi v_F}\mathrm{Im}\left[\int_0^{\tilde{\chi}^0_{\mathrm{SDW}}(\mathbf{q}+\mathbf{q}_0,\omega)} \langle z^2_{\mathrm{SDW}}(k_b)\rangle d\ell\right] \\ &= \chi_{\mathrm{SDW}}(\mathbf{q}_0)\mathrm{Im}[1-\xi_a^2q^2-\xi_b^2q_b^2 \\ &\quad -\xi_c^2(\sin q_c)^2+i\Gamma\omega+\cdots]. \end{aligned} \tag{A1}$$

This expression will be equated with the expansion of

$$\mathrm{Im}\,\chi_{\mathrm{SDW}}(\mathbf{q}+\mathbf{q}_0,\omega) \simeq \mathrm{Im}\left[\frac{\chi_{\mathrm{SDW}}(\mathbf{q}_0)}{1+\xi_a^2q^2+\xi_b^2q_b^2+\xi_c^2(\sin q_c)^2-i\Gamma\omega}\right] = \frac{\chi_{\mathrm{SDW}}(\mathbf{q}_0)\Gamma\omega}{[1+\xi_a^2q^2+\xi_b^2q_b^2+\xi_c^2(\sin q_c)^2]^2+\Gamma^2\omega^2}, \tag{A2}$$

which we shall use in the following. Here $\xi_i^2=\xi_{0,i}^2\langle z^2_{\mathrm{SDW}}(k_b)\rangle/\tilde{\chi}_{\mathrm{SDW}}$, is the square of correlation length along $i=a$, b, and c directions; $\xi_{0,i}$ are the corresponding coherence lengths evaluated at the SDW temperature $T_0\simeq 12$ K obtained for small $t'_{\perp b}$, that is

$$\xi_{0,i}^2 = -\left(\frac{v_i}{2\pi T_0}\right)^2 \mathrm{Re}\left\{\int_0^{\pi/2}\frac{dk_b}{2\pi}\psi'\left[\frac{1}{2}-i\frac{t'_{\perp b}}{\pi T_0}\cos(2k_b)\right]\right\}, \tag{A3}$$

where $v_a=v_F/\sqrt{2}$ and $v_{b,c}=t_{\perp b,c}$. The relaxation time for SDW fluctuations is $\Gamma=\Gamma_0\langle z^2_{\mathrm{SDW}}(k_b)\rangle/\tilde{\chi}_{\mathrm{SDW}}$, where Γ_0 is a characteristic short-range time scale at short distance, which is given by

$$\Gamma_0 = \frac{1}{\pi T_0}\mathrm{Re}\left\{\int_0^{\pi/2}\frac{dk_b}{2\pi}\psi'\left[\frac{1}{2}-i\frac{t'_{\perp b}}{\pi T_0}\cos(2k_b)\right]\right\}. \tag{A4}$$

Substituting the imaginary part Eq. (A1) in the expression for the antiferromagnetic component of the nuclear relaxation rate, Eq. (10), we get in the limit $\omega\to 0$

$$\begin{aligned} T_1^{-1}(\mathbf{q}\sim\mathbf{q}_0) &= 8T|A_{\mathbf{q}_0}|^2\int_0^{\xi_{0,a}^{-1}}\int_0^{\xi_{0,b}^{-1}}\int_0^{\pi}\frac{\mathrm{Im}\,\chi(\mathbf{q},\omega)}{\omega}dqdq_bdq_c \\ &= 8\pi|A_{\mathbf{q}_0}|^2T[N(E_F)]^2\tilde{\chi}_{\mathrm{SDW}}(\mathbf{q}_0)\frac{v_F\Gamma_0}{\xi_{0,a}\xi_{0,b}}\int_0^{\sqrt{r/\alpha}}\int_0^{\sqrt{r/\alpha}}\int_0^{\pi}\frac{dxdydq_c}{(1+x^2+y^2+\xi_c^2(\sin q_c)^2)^2} \\ &= 2\pi^3|A_{\mathbf{q}_0}|^2T[N(E_F)]^2\tilde{\chi}_{\mathrm{SDW}}(\mathbf{q}_0)\frac{v_F\Gamma_0}{\xi_{0,a}\xi_{0,b}}\left[\frac{1}{\sqrt{1+\xi_c^2}}-\frac{1}{\sqrt{(1+r)(1+r+\xi_c^2)}}\right]. \end{aligned} \tag{A5}$$

Here $r=\alpha\langle z^2_{\mathrm{SDW}}(k_b)\rangle/\tilde{\chi}_{\mathrm{SDW}}$ and $\alpha\simeq 1.114$ is a constant introduced to adjust the upper bound cutoff in order to go through a polar integration in the ab plane. This allows an analytical expression to be found that deviates from the numerical (rectangular) integration by less than 0.1%.

2. Uniform part

Following Eq. (10), the uniform component of the relaxation rate is given by

$$T_1^{-1}(q\sim 0) = T|A_0|^2\int_{q\sim 0}\frac{\mathrm{Im}\,\chi(\mathbf{q},\omega)}{\omega}\frac{d^3q}{(2\pi)^3}. \tag{A6}$$

Using an RPA expression for the dynamical spin susceptibility at small q and ω, we have for the imaginary part

$$\mathrm{Im}\,\chi(\mathbf{q},\omega) = -\eta^2\frac{2}{LN_\perp}\sum_{\mathbf{k}}\sum_p \mathrm{Im}\left\{\frac{n[E_p(\mathbf{k}+\mathbf{q})]-n[E_p(\mathbf{k})]}{E_p(\mathbf{k}+\mathbf{q})-E_p(\mathbf{k})-\omega-i0^+}\right\}, \tag{A7}$$

where $\eta=(1-\lambda)^{-1}$ is an enhancement factor from interaction parameterized by $\lambda<1$. For ω and q going to zero, we have in the low-temperature limit

$$\begin{aligned}\mathrm{Im}\,\chi(\mathbf{q},\omega)|_{\omega,q\to 0} &= -\eta^2\frac{1}{4\pi^2}\sum_p\int\int dE_p\frac{dS_E}{|\nabla E_p(\mathbf{k})|}\{n[E_p(\mathbf{k})+\omega]-n[E_p(\mathbf{k})]\}\delta[\omega-E_p(\mathbf{k}+\mathbf{q})+E_p(\mathbf{k})],\\ &= \eta^2\frac{\omega}{4\pi^2}\sum_p\int\frac{dS_F}{|\nabla E_p(\mathbf{k}_F)|}\delta[E_p(\mathbf{k}_F+\mathbf{q})-E_p(\mathbf{k}_F)]. \qquad \text{(A8)}\end{aligned}$$

Only a constant (Fermi) surface integral remains. The substitution in Eq. (A6), allows one to write

$$T_1^{-1}(q\sim 0)=\frac{T}{(2\pi)^5}|A_0|^2\eta^2\sum_p\int d^3q\int\frac{dS_F}{|\nabla E_p(\mathbf{k}_F)|}\delta[E_p(\mathbf{k}_F+\mathbf{q})-E_p(\mathbf{k}_F)]=\frac{2T}{(2\pi)^5}|A_0|^2\eta^2\left[\int\frac{dS_F}{|\nabla E_p(\mathbf{k}_F)|}\right]^2. \qquad \text{(A9)}$$

Using the approximation $|\nabla E_p(\mathbf{k}_F)|\approx v_F$ for $t_{\perp c}\ll t_{\perp b}\ll v_F$, and $\int dS_F=4\pi^2$, one obtains the Korringa component

$$T_1^{-1}(q\sim 0)=\pi|A_0|^2[N(E_F)]^2\eta^2T. \qquad \text{(A10)}$$

[1] D. Jérome and H. Schulz, Adv. Phys. **31**, 299 (1982).
[2] C. Bourbonnais and D. Jérome, in *The Physics of Organic Superconductors and Conductors*, Springer Series in Materials Science Vol. 110, edited by A. Lebed (Springer, Heidelberg, 2008), p. 357.
[3] S. E. Brown, P. M. Chaikin, and M. J. Naughton, in *The Physics of Organic Superconductors and Conductors*, Springer Series in Materials Science Vol. 110, edited by A. Lebed (Springer, Heidelberg, 2008), p. 49.
[4] C. Bourbonnais, F. Creuzet, D. Jérome, K. Bechgaard, and A. Moradpour, J. Phys. (Paris), Lett. **45**, L755 (1984).
[5] F. Creuzet, C. Bourbonnais, L. G. Caron, D. Jérome, and A. Moradpour, Synth. Met. **19**, 277 (1987).
[6] M. Takigawa and G. Saito, J. Phys. Soc. Jpn. **55**, 1233 (1986).
[7] P. Wzietek, F. Creuzet, C. Bourbonnais, D. Jérome, K. Bechgaard, and P. Batail, J. Phys. I **3**, 171 (1993).
[8] W. Wu, P. M. Chaikin, W. Kang, J. Shinagawa, W. Yu, and S. E. Brown, Phys. Rev. Lett. **94**, 097004 (2005).
[9] J. Shinagawa, Y. Kurosaki, F. Zhang, C. Parker, S. E. Brown, D. Jérome, K. Bechgaard, and J. B. Christensen, Phys. Rev. Lett. **98**, 147002 (2007).
[10] F. Creuzet, D. Jérome, and A. Moradpour, Mol. Cryst. Liq. Cryst. (Phila. Pa.) **119**, 297 (1985).
[11] T. Takahashi, D. Jérome, and K. Bechgaard, J. Phys. (Paris) **45**, 945 (1984).
[12] F. Creuzet, D. Jérome, C. Bourbonnais, and A. Moradpour, J. Phys. C **18**, L821 (1985).
[13] C. S. Jacobsen, D. B. Tanner, and K. Bechgaard, Phys. Rev. Lett. **46**, 1142 (1981).
[14] J. Moser, M. Gabay, P. Auban-Senzier, D. Jérome, K. Bechgaard, and J. M. Fabre, Eur. Phys. J. B **1**, 39 (1998).
[15] V. Vescoli, L. Degiorgi, W. Henderson, G. Gruner, K. P. Starkey, and L. Montgomery, Science **281**, 1181 (1998).
[16] A shorter version of this work has been given by C. Bourbonnais and A. Sedeki, Proceedings of the International Symposium on Molecular Conductors (ISMC 2008), Ogazaki, Japan, July 2008; J. Phys.: Conf. Ser. **132**, 012017 (2008).
[17] R. Duprat and C. Bourbonnais, Eur. Phys. J. B **21**, 219 (2001).
[18] J. C. Nickel, R. Duprat, C. Bourbonnais, and N. Dupuis, Phys. Rev. B **73**, 165126 (2006).
[19] I. E. Dzyaloshinskii and A. I. Larkin, Sov. Phys. JETP **34**, 422 (1972).
[20] V. J. Emery, R. Bruinsma, and S. Barisic, Phys. Rev. Lett. **48**, 1039 (1982).
[21] T. Giamarchi, *Quantum Physics in One Dimension* (Oxford University Press, Oxford, 2004).
[22] P. M. Grant, Phys. Rev. B **26**, 6888 (1982).
[23] L. Ducasse, A. Abderraba, J. Hoarau, M. Pesquer, B. Gallois, and J. Gaultier, J. Phys. C **19**, 3805 (1986).
[24] D. Le Pévelen, J. Gaultier, Y. Barrans, D. Chassau, F. Castet, and L. Ducasse, Eur. Phys. J. B **19**, 363 (2001).
[25] S. Barisic and S. Brazovskii, in *Recent Developments in Condensed Matter Physics*, edited by J. T. Devreese (Plenum, New York, 1981), Vol. 1, p. 327.
[26] K. Penc and F. Mila, Phys. Rev. B **50**, 11429 (1994).
[27] C. Bourbonnais, J. Phys. I **3**, 143 (1993).
[28] Y. Fuseya, M. Tsuchiizu, Y. Suzumura, and C. Bourbonnais, J. Phys. Soc. Jpn. **76**, 014709 (2007).
[29] N. Miljak and J. R. Cooper, Mol. Cryst. Liq. Cryst. **119**, 141 (1985).
[30] N. Miljak, J. R. Cooper, and K. Bechgaard, J. Phys. Colloq. **44**, C3-893 (1983).
[31] For anisotropic two-dimensional electron systems, T_μ is a scale for the onset of short-range order in the channel μ. True long-range order, at a temperature nevertheless close to T_μ, is assured by the finite interchain hopping $t_{\perp c}$ along the c direction.
[32] In the theory of the one-dimensional electron-gas model, for example, the presence of short-range superconductive fluctuations is detrimental to Umklapp scattering. Attractive interactions couple negatively to g_3, which then becomes a marginally irrelevant variable as spin fluctuations are suppressed. See, for example, Ref. 21 and J. Solyom, Adv. Phys. **28**, 201 (1979).
[33] T. Moriya, J. Phys. Soc. Jpn. **18**, 516 (1963).
[34] Y. Fuseya, M. Tsuchiizu, Y. Suzumura, and C. Bourbonnais, J. Phys. Soc. Jpn. **74**, 3159 (2005).
[35] C. Bourbonnais, P. Wzietek, F. Creuzet, D. Jérome, P. Batail, and K. Bechgaard, Phys. Rev. Lett. **62**, 1532 (1989).
[36] The relative smallness of $|A_{\mathbf{q}_0}|$ may have its origin from the presence of an oscillating factor $e^{i\mathbf{q}_0\cdot\mathbf{r}}$ in the evaluation of this hyperfine matrix element at large momentum transfer.
[37] B. Horovitz, H. Gutfreund, and M. Weger, Phys. Rev. B **12**, 3174 (1975).
[38] K. Yamaji, J. Phys. Soc. Jpn. **51**, 2787 (1982).
[39] T. Moriya, Y. Takahashi, and K. Ueda, J. Phys. Soc. Jpn. **59**, 2905 (1990).
[40] N. Doiron-Leyraud, P. Auban-Senzier, S. René de Cotret, R. Homier, A. Sedeki, C. Bourbonnais, D. Jérome, K. Bechgaard, and L. Taillefer (unpublished) arXiv:0905.0964.